SURFACE PHYSICS

Vacuum-tunneling spectroscopy

The extension into the vacuum of the exponential tail of the wave function makes possible remarkably sensitive techniques based on field emission, ion neutralization and field ionization.

E. Ward Plummer, John W. Gadzuk and David R. Penn

Any spectroscopy that is to be used to study surfaces must be sensitive, almost specific to the surface. The most successful surface spectroscopies, whether they measure emission or absorption spectra of electrons, can be grouped into two general categories depending upon the origin of their surface sensitivity. The first group, which includes photoemission, Auger and appearance-potential spectroscopy, owes its surface sensitivity to the strong electron–electron interactions of an incoming or outgoing electron, which limits the inelastic mean free path of an unscattered electron to at most a few atomic layers in the appropriate range of electron energy. The second group of electron spectroscopies, which is the subject of this article, derive their surface sensitivity from a sampling of the exponential tails of the wave functions, which tunnel into the vacuum. We have called this set of experimental techniques "vacuum-tunneling spectroscopy."

We will discuss three such tunneling spectroscopies in this article; the appropriate energy level diagrams for them are shown in figure 1. In *field-emission spectroscopy* we measure the distribution of the kinetic energies of electrons that tunnel from the solid into the vacuum when a large electrostatic field is applied. In *ion-neutralization spectroscopy* we measure the kinetic-energy distribution of electrons ejected from the solid by a radiationless Auger-type transition that neutralizes a slowly moving positive ion (usually He^+) just outside of the surface. This is a two-electron process: One electron tunnels from the solid to the ion and drops into the ground state of the atom; a second electron from the solid accepts the energy released by the downward transition of the first electron and is ejected from the solid.

The third tunneling spectroscopy shown in figure 1 is *field-ionization spectroscopy*. In this process a neutral atom, usually helium or neon, is ionized near the surface in the presence of a large electric field, which is opposite in polarity to the field used in field emission. The electron in the ground state of the neutral He atom tunnels into an unoccupied state in the solid, leaving the helium atom singly ionized. These ions are then accelerated away from the surface and subsequently energy analyzed. For a fixed applied voltage, the final kinetic energy of the ion will be determined by the distance from the surface at which ionization occurred. Therefore, if the field is known, the kinetic energy of the ion can be related to the energy of the state at the surface into which the helium atom's electron has tunneled.

Why are vacuum-tunneling spectroscopies sensitive only to the surface? These techniques measure the number j of electrons tunneling at energy ϵ per unit time; this current can be calculated from the golden rule,

$$j(\epsilon) = (2\pi/\hbar)\sum_{if} |\langle \Psi_i|V'|\Psi_f\rangle|^2 \times \delta(E_i - E_f)\delta(\epsilon - E_f) \quad (1)$$

Here Ψ_i is the wave function of the initial state of the electron, prior to tunneling and Ψ_f is the final state, after the vacuum-tunneling event. The first delta function insures that we include only matrix elements for which the energy is conserved, and the second delta function picks out only those electrons that emerge with energy ϵ.

The processes of field emission and field ionization are easily visualized in equation 1. In both of these cases the "external perturbation" V' is just the applied electric potential. In the case of field emission Ψ_i is the bulk wave function and Ψ_f the vacuum wave function; see part a of figure 1. In field ionization, part c, Ψ_i is the helium 1s wave function and Ψ_f the bulk wave function of the substrate. In both cases, $j(\epsilon)$ depends upon the overlap of Ψ_i and Ψ_f outside the metal. In this region, both Ψ_i and Ψ_f are decaying exponentially—in opposite directions.

For field emission, Ψ_f is a known function, so that $j(\epsilon)$ is sensitive to the exponential tails of Ψ_i in the vacuum, which are dictated by the highly local properties of Ψ_i at the surface. In the case of field ionization, on the other hand, Ψ_i is known, so that $j(\epsilon)$ samples the exponential tails of the bulk wave functions for the unoccupied states above the Fermi energy.

The tunneling spectroscopies therefore effectively have no depth perception into the solid. If a bulk property does not affect the wave functions "at the surface," they will not see it.

Field-emission spectroscopy

Field emission is achieved by applying a large electrostatic field, approximately 30 million V/cm, to a cold cathode so that electrons can tunnel from the solid through the classically forbidden barrier into the vacuum.[1] To obtain these high fields with reasonable voltages, the cathode or emitter is usually etched to a sharp point (about 1000 Å in radius). Therefore, several thousand volts will produce the desired field. Erwin Müller[2] realized in 1937 that if this hemispherically shaped emitter were cleaned thermally, a greatly enlarged (over 10^6 times) image of the spatial distribution of the tunneling electrons could be projected onto a fluorescent screen.

The tip of the emitter exposes all crystallographic orientations, so that the individual crystal planes can be located and identified in the field-emission pattern observed on the fluorescent screen. The emission characteristics of any crystal plane may be studied by placing a small "probe hole" in the screen and deflecting the field-emission pattern with electrostatic deflection

E. Ward Plummer is associate professor of physics at the University of Pennsylvania; John W. Gadzuk and David R. Penn are physicists at the Surface and Electron Physics Section of the National Bureau of Standards.

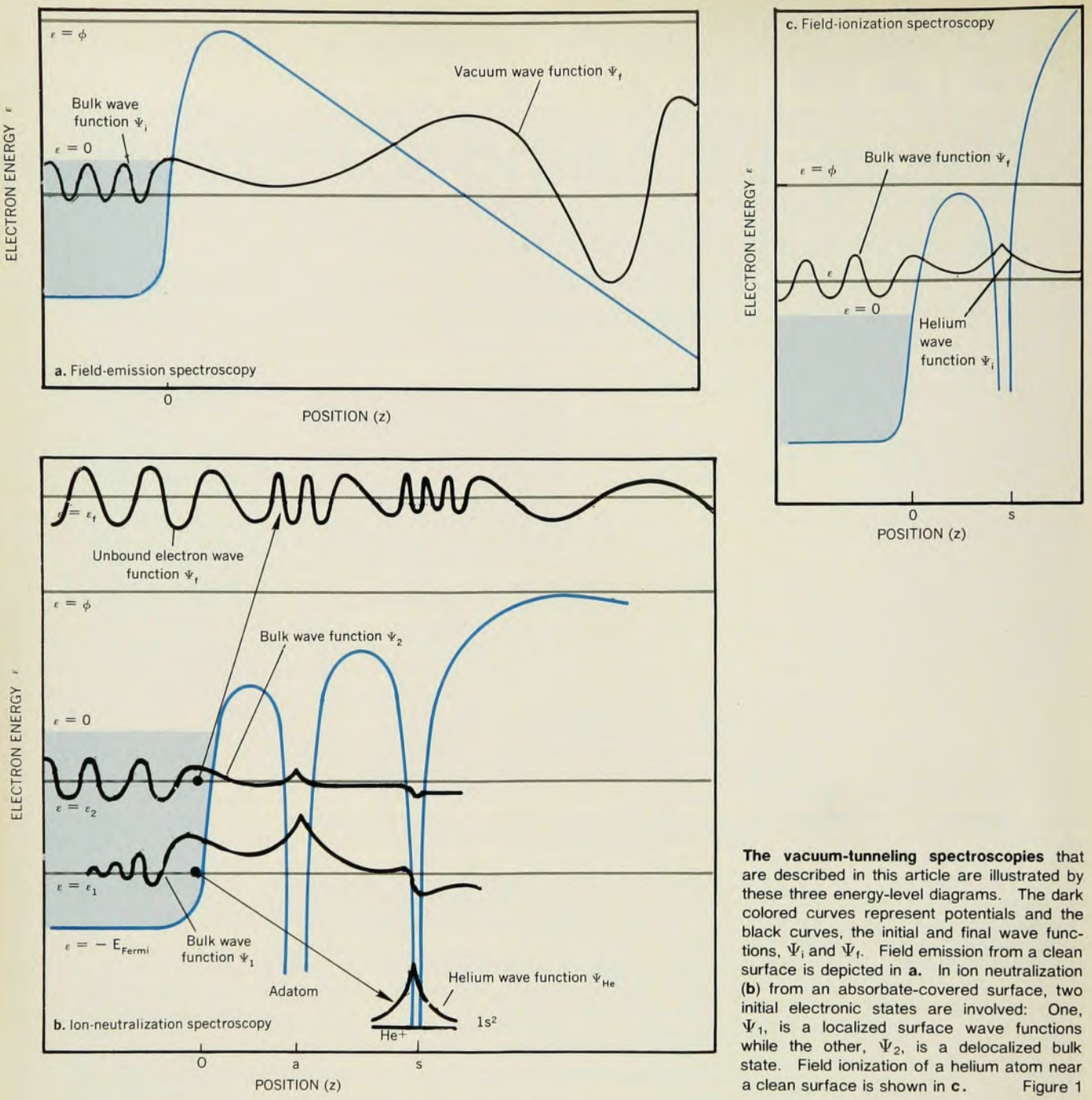

The vacuum-tunneling spectroscopies that are described in this article are illustrated by these three energy-level diagrams. The dark colored curves represent potentials and the black curves, the initial and final wave functions, Ψ_i and Ψ_f. Field emission from a clean surface is depicted in **a.** In ion neutralization (**b**) from an absorbate-covered surface, two initial electronic states are involved: One, Ψ_1, is a localized surface wave functions while the other, Ψ_2, is a delocalized bulk state. Field ionization of a helium atom near a clean surface is shown in **c.** Figure 1

plates until the plane of interest is over the probe hole. The properties of the electrons passing through the probe hole may then be measured. Figure 2 is a schematic drawing of this arrangement, showing the field emitter (tip) on a support loop and the projected field emission pattern of clean tungsten on the screen. In this figure, the (110) plane is positioned over the probe hole and the electrons passing through the probe hole are being analyzed. The field dependence of the total current can also be measured to obtain changes in the work function.

The phenomenon of field emission was the first tunneling process in a bulk system to which quantum mechanics was applied. In 1928, Ralph Fowler and Lothar Nordheim[3] calculated the emitted current density J from a free-electron metal with a work function φ, terminated by a step barrier at the surface and a constant applied field F outside of the metal. Their result,

$$J = (CF^2/\varphi)\exp[-(4/3e\hbar F)(2m\varphi^3)^{1/2}]$$

is known as the Fowler–Nordheim equation. This equation is still commonly used to measure work-function changes by measuring the change in the slope of a plot of $\log(J/F^2)$ versus $1/F$. The probe-hole arrangement shown in figure 2 can be used to measure work-function changes from the individual crystal planes of the emitter.

In 1959, Russell Young[4] showed theoretically and experimentally that the energy distribution of electrons emerging from the probe hole for a free-electron metal is

$$j_0'(\epsilon) = Bf(\epsilon)\exp[-(2\epsilon/e\hbar F)(2m\varphi)^{1/2}] \quad (2)$$

where ϵ is the energy measured from the Fermi energy and $f(\epsilon)$ is the Fermi–Dirac distribution function. Therefore, the field-emission energy distribution will decrease exponentially as the energy decreases and will be cut off at the Fermi energy by the Fermi–Dirac distribution of electrons. For a typical case, with $\varphi = 4.5$ eV and $F = 30 \times 10^6$ V/cm, the $1/e$ falloff of the energy distribution occurs at an energy of about 0.15 eV. A field-emission electron gun therefore furnishes a very monochromatic source of electrons.

The exponential nature of the field-emission energy distribution $j_0'(\epsilon)$ is a consequence of the increasing size of the barrier through which an electron with lower energy must tunnel, as figure 1a shows. Since this barrier is almost entirely in the vacuum, very little information about the electronic states of the surface is contained in the exponential shape of the energy distribution. Instead it is the pre-exponential terms that contain the details of the surface wave function, the information desired.

The probability an electron of energy ϵ has to tunnel through a vacuum barrier characterized by a field F and a work function φ must be calculated and the measured energy distribution $j'(\epsilon)$ divided by this "free-electron" energy distribution[5] $j_0'(\epsilon)$, in order to eliminate the exponential dependence on ϵ. If the work function is obtained from an independent measurement, the measured Fowler–Nordheim plot can be used to calculate the field F and a more accurate expression than given in equation 2 can be used to calculate $j_0'(\epsilon)$.

Figure 3 illustrates the procedure for obtaining the measured energy distribution $j'(\epsilon)$ from the (100) surface of tungsten at 77 K. The ratio of the pre-exponentials is defined as

$$R(\epsilon) \equiv j'(\epsilon)/j_0'(\epsilon) \qquad (3)$$

Since there are pre-exponential constants in $j_0'(\epsilon)$ that we do not calculate, $R(\epsilon)$ has been normalized to 1.0 at $\epsilon = -1.0$ eV. The $R(\epsilon)$ curves exhibit quite a pronounced structure, which is different for each crystal face of tungsten,[5] and quite different for other substrates such as germanium[6] and iridium.[7]

The field-emission barrier is a well prescribed one-dimensional vacuum barrier. Therefore, it is straightforward to calculate Ψ outside the surface. This allows us to relate the properties of the measured energy distribution to the properties of the wave function by a two-dimensional integral over the surface[7] $z = 0$.

$$R(\epsilon) \propto \rho_\perp(\epsilon, 0) = \int \rho_\perp(\epsilon, \mathbf{r})ds$$

where $\rho_\perp$ is the one-dimensional density of states perpendicular to this surface. It is evaluated at $z = 0$, which is the point at which a classical particle would be turned back by the barrier. The field-emission data analyzed in this fashion provide a very direct measurement of the density of states at the surface.

The curve shown in figure 3 is a very interesting case, since the large peak in $\rho_\perp$ at an energy 0.35 eV below the Fermi energy has no counterpart in the bulk one-dimensional density of states. It represents a large density of states at the surface, which may be either a surface state or a surface resonance. This structure in the one-dimensional density of states is extremely sensitive to the surface conditions. It is usually removed with submonolayer adsorption of anything that has ever been studied, from chemisorbed gases such as H_2 and CO to physically adsorbed gases such as Xe and Kr. The measured field-emission curve for the tungsten (100) face with one third of a monolayer of hydrogen is also shown in figure 3.

Detection of single atoms

The structure in the field-emission energy distribution is very sensitive to the adsorption of foreign atoms or molecules. In 1967 Charles Duke and M. E. Alferieff[9] showed that the tunneling of electrons through an adsorbate is a resonance phenomenon; that is, when the electron that is tunneling from the solid has the same energy as a bound state in the adsorbate, resonance will occur, increasing the tunneling probability 100–10 000 times. This enhancement in the tunneling probability as a function of energy can be used to measure the local density of states on the adsorbed atom or molecule.[5] In this case, the $R(\epsilon)$ curves are given by

$$R(\epsilon) \propto \rho_A = \int \rho(\epsilon, \mathbf{r})dV$$

where the integral is over the volume of the atom.

Figure 4 dramatically illustrates the sensitivity of field-emission specttroscopy to the presence of an adsorbed atom on a single crystal face of the substrate. The total current through the probe hole was monitored as strontium was deposited on a tungsten tip. Because of the magnification of the microscope and the small size of the probe hole, only about 30 surface atoms on the desired crystal face are projected over the probe hole. Some interval after the strontium evaporator was turned on, a strontium atom arrived within the area of the surface sampled by the probe hole. The current jumped by about 40%, and the evaporator was turned off. Thus we are able to record the effect of a single atom on the energy distribution of an atomically defined crystal plane. In fact, this was done for single adsorbed atoms of barium, strontium and calcium on four low-index faces of tungsten.[10] Figure 4 also shows the arrival of a second strontium atom, which resulted in an even larger increase in the current, presumably because it was closer to the center of the probe hole than the first strontium atom.

There is another important aspect of field-emission tunneling with an adsorbed atom or molecule on the surface. A tunneling electron may undergo an inelastic collision with an adsorbed molecule. The inelastically scattered electron will appear in the energy distribution with its energy reduced by the excitation energy $\hbar\omega_p$. Since at low temperatures the Fermi energy produces a sharp cutoff in the maximum initial energy, the $R(\epsilon)$ curves will display a threshold step at energies $\hbar\omega_p$ below the Fermi energy, where $\hbar\omega_p$ is again the characteristic loss energy of the surface complex. The total cross section for such an inelastic process will be

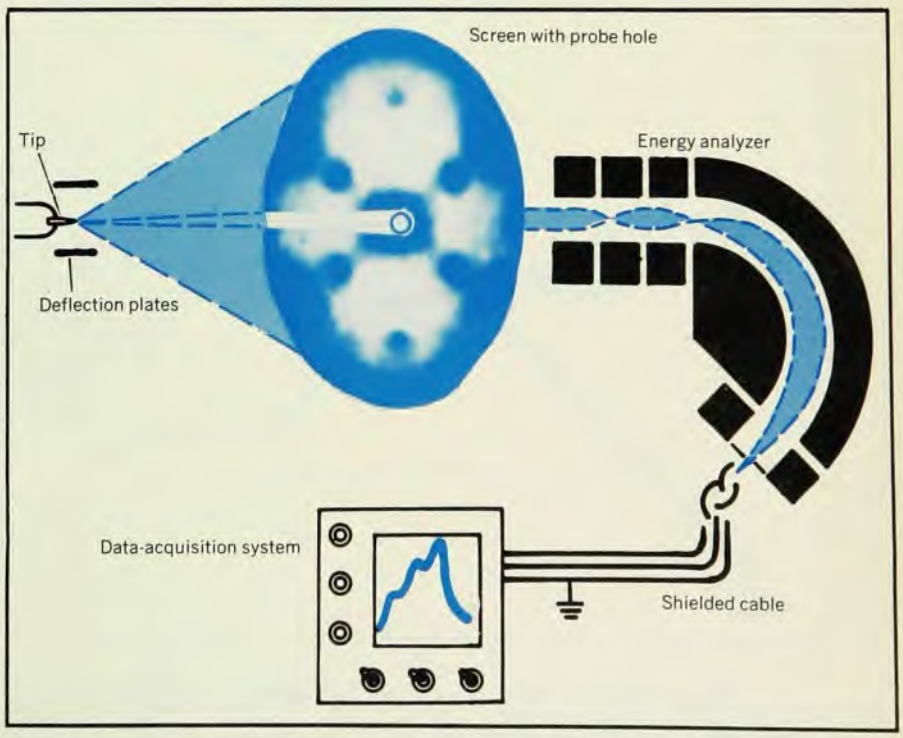

A field-emission microscope adapted to make energy-distribution measurements. Electrons emitted from the plane of interest are sampled by means of a probe hole in a screen. The field-emission pattern shown is that of the (110) plane of clean tungsten. Figure 2

small. Consequently, the structure in the $R(\epsilon)$ curves due to inelastic scattering will usually be much smaller than that due to resonant tunneling.[11]

Figure 5 shows the observed vibrational frequencies of hydrogen and deuterium adsorption on the (111) face of tungsten at 77 K. The lower curve is for adsorption of deuterium at 77 K in an amount equivalent to approximately two monolayers of deuterium atoms. There are undoubtedly multiple states of binding but at least one of them is molecular: We observe a vibrational loss at −0.43 eV, which is the stretch frequency of the D_2 molecule. The solid circles show the equivalent stretching frequency for adsorbed hydrogen to be at an energy of −0.55 eV, which corresponds to the appropriate $\sqrt{2}$ shift. The additional vibrational modes indicated on the deuterium curve by the arrows are vibrational modes of the hydrogen–tungsten surface complex. When the substrate is warmed to 200 K, some deuterium is desorbed. The vibrational loss at 0.4 eV disappears, indicating that the molecularly bound D_2 has been desorbed and the remaining deuterium is adsorbed as atoms. The upper curve of figure 5 shows this ratio for hydrogen adsorption at 200 K.

The limitations of field-emission spectroscopy are twofold: Due to the exponential nature of the spectrum, there is a practical limitation on the energy range that is accessible, of less than about 3 eV; and there are a limited number of molecules that are suitable for use as emitters. Among the advantages are the high degree of surface sensitivity and our ability to interpret the data.

Ion-neutralization spectroscopy

The second type of vacuum-tunneling spectroscopy to be considered is ion-neutralization spectroscopy.[12] This technique was pioneered by Homer D. Hagstrum at Bell Labs and has been extensively utilized by Hagstrum and Gordon Becker in conjunction with other *in situ* experimental probes (ultraviolet photoelectron spectroscopy, LEED, Auger), to study both electronic structure and fundamental electron processes at surfaces. The basic mechanism of ion-neutralization spectroscopy is the Auger effect, which is a radiationless decay involving two electrons. The initial vacancy or hole is provided by a low-energy ion beam, usually helium, directed onto the surface as shown in figure 1. The substrate is represented by a potential well of depth $E_f + \varphi_e$ where E_f is the width of the occupied portion of the conduction band and φ_e is the surface work function. The He^+, a distance s from the surface, is represented by the Coulomb well with a ground-state ionization energy E_{He}.

The two electrons that interact in the ion-neutralization process come from occupied states in the metal. These may be delocalized sums of Bloch band states such as Ψ_2 in figure 1b, or they may be localized surface states, either intrinsic or extrinsic due to chemisorbed atoms, as pictured by Ψ_1 in the figure. Their interaction via their electron–electron repulsion results in an energy-conserving, nonradiative transition. The final state is one in which one of the electrons fills the vacant state Ψ_{He} in the He^+, while the other electron is excited to a continuum state Ψ_f, which is at an energy sufficiently high to pass over the surface work-function barrier. It is these electrons that are then energy analyzed, giving an ion-neutralization spectrum.

The tunneling aspect of the ion-neutralization process is best illustrated by examining the INS matrix element[12]

$$M_{if} = \int d^3r_1 \Psi_f^*(\mathbf{r}_1) \left| \int d^3r_2 \Psi_{He}^*(\mathbf{r}_2) (e^2/r_{12}) \times \Psi_1(\mathbf{r}_2) \right| \Psi_2(\mathbf{r}_1) \quad (4)$$

Since both initial-state wave functions Ψ_1 and Ψ_2 are bound states, they extend into the vacuum half-space $z > a$ only to the extent that they have exponentially decaying tails that tunnel out. From physical considerations, the He^+ is always constrained to remain in the $z > a$ domain. Thus the strength of the Auger decay depends on the overlap of the Ψ_1 tunneling tail with Ψ_{He}, as seen in the bracketed integral in equation 4. Furthermore, the effective potential given by this integral falls off roughly inversely with distance from the ion core; thus the form of Ψ_2 in the surface region is also sensed in the INS process.

In all cases, ion-neutralization spectroscopy mainly probes states that are localized at the surface, or the detailed features of Bloch states that may be distorted in the surface region. In fact, INS was the first experiment in which virtual states associated with chemisorbed atoms were observed.[13]

Some insight into the spatial localization and directionality of the ion-neutralization probe can be gained by further consideration of equation 4. If, for example, the state Ψ_1 corresponded to an orbital in an adsorbate such as a p orbital in a chalcogen, then the p_z orbital would have much greater overlap with Ψ_{He} than would the p_x or p_y orbitals and thus would be much more visible in the ion-neutralization spectra. Likewise, an adsorbed atom embedded interstitially in the surface layer would have a smaller INS matrix element compared to the case of the atom on the surface. This distinction would not be nearly so great in a photoemission experiment; see the article by Dean Eastman and Marshall Nathan in this issue. This selectivity can be used to advan-

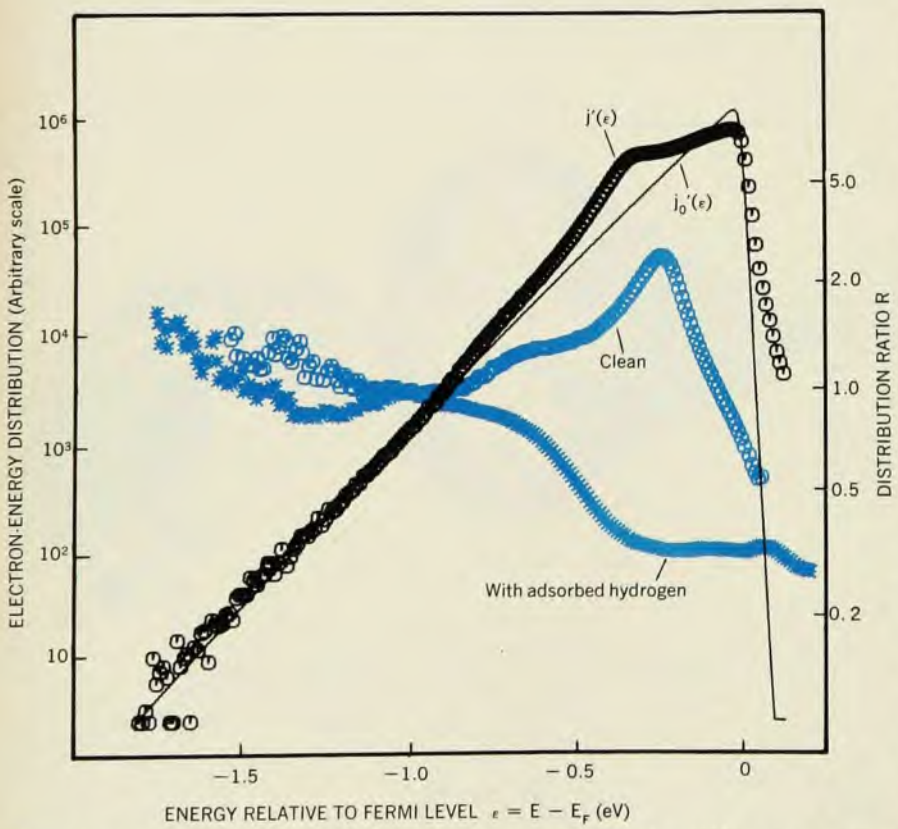

Energy distribution $j'(\epsilon)$ of electrons field-emitted from a clean tungsten (100) surface at 77 K and a 3.52 × 10^7 V/cm field (black circles) and calculated free-electron distribution $j_0'(\epsilon)$ (black line) for a work function of 4.64 eV. Their ratios R (color, right-hand scale) are shown for a clean surface and one with about 1/3 monolayer of hydrogen. Figure 3

Find out how RCA can fill your PMT needs.

It's easy! Ask our applications engineers, marketing managers, or phototube (PMT) distributors. They'll all tell you how RCA's PMTs and Integrated Photodetection Assemblies (IPAs) excel in quality, reliability, and performance.

These PMTs offer characteristics such as nanosecond rise time, high temperature operation, low noise, and high spectral sensitivity from the UV to the near IR.

Cap these performance characteristics with tough quality assurance testing . . . and you'll know why RCA PMTs can save you design dollars.

And users know, too, that RCA for 40 years continues to be the industry's leading supplier of PMTs. They'll tell you that with a line of 200 PMTs in all standard sizes, RCA offers the industry a variety of PMTs that is second to none in depth. That's why RCA should be your first choice as the source for your PMT requirements.

RCA PMTs are available through your RCA Representative or your RCA Industrial Tube Distributor. Or, complete and return the reply coupon below.

Spectroscopy
- 931B
- 1P28B

Medical Electronics
- 4523
- 4524/V4

Scintillation Counting
- 6199
- 6342A/V1
- 4856

Laser Ranging
- 4836
- 8644

Photon Counting
- C31034
- C31034A

Oil Well Logging
- C31000AJ
- C31061A
- C31059A

Pollution Monitoring
- 8852
- 4836
- 4507

High Energy Physics
- 8575
- 8850
- 8854

RCA Lancaster — where people and technology make the difference.

Manager, Phototube Marketing
RCA, New Holland Avenue
Bldg. 100
Lancaster, Pa. 17604

Please send me your selection guide and more information on the following RCA Phototubes _____

119D

Please Print. This is your mailing label.

Name _____

Company _____

Street _____

City _____

State _____ Zip _____

RCA Phototubes

INTERNATIONAL SALES OFFICES: ARGENTINA – Casilla de Correo 4400 Buenos Aires/BRAZIL – Caixa Postal 30433, São Paulo/CANADA – 21001 No. Service Rd., Ste. Anne de Bellevue, 810 Quebec/ENGLAND – Sunbury-on-Thames, Middlesex/HONG KONG – P.O. Box 112/MEXICO – Apartado 17-570, Mexico 17, D.F./SWITZERLAND – 118 rue du Rhone CH1204, Geneva

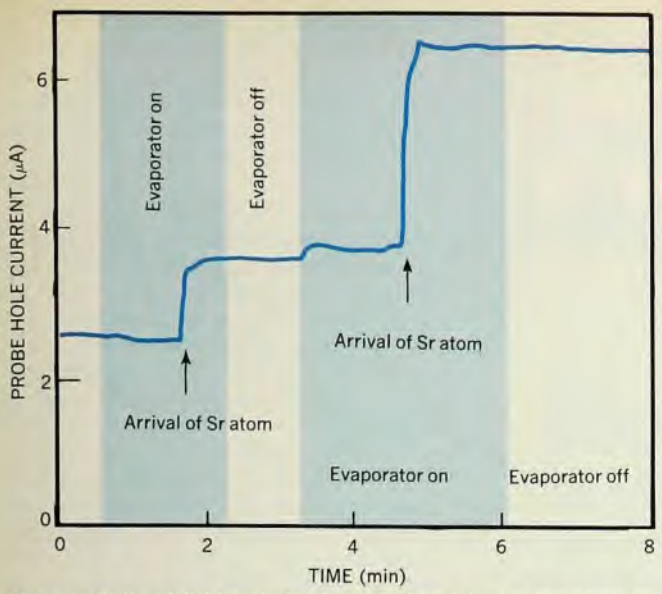

The sensitivity of field emission to a single adatom is illustrated by the time variation of the probe-hole current when a strontium evaporation source is turned on (colored strips) and off. The experimental arrangement is similar to that shown in figure 2. The step increase in current, a resonance phenomenon, signals the arrival of a single strontium atom upon the tungsten surface being viewed. (From H. E. Clark and R. D. Young, reference 10.) Figure 4

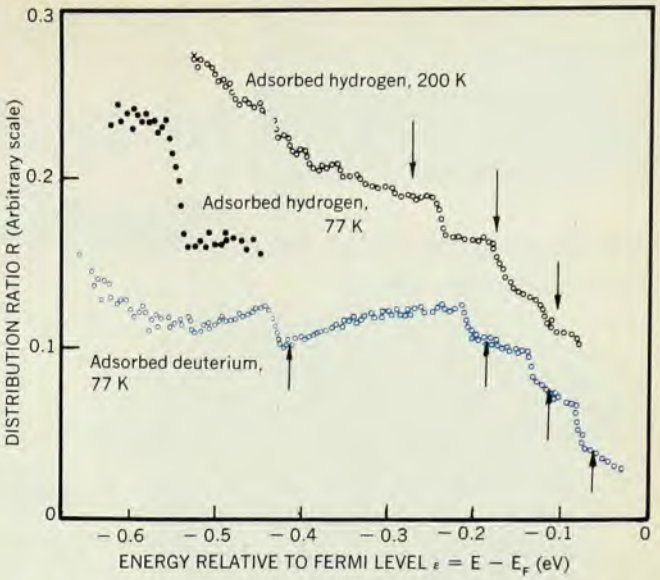

The effects of inelastic tunneling are visible in these curves of distribution ratios for adsorbed hydrogen and deuterium. Arrows indicate threshold energies at which vibrational modes of the surface complex are excited by electrons. Deuterium, adsorbed to saturation at 77 K, shows its molecular vibration mode at about −0.4 eV, and hydrogen, −0.55 eV. At 200 K, molecules are desorbed. The other losses indicated are due to H- and D-tungsten complexes. Figure 5

tage when INS is used in conjunction with other spectroscopic probes, since it can enable one to differentiate between alternative bond sites and orbital directions.

The Auger process, which is fundamental to ion-neutralization spectroscopy, is a two-electron process and as a result, INS would appear to be much more complicated than one-electron spectroscopies such as field- and photoemission. The observed energy distribution is of the form

$$N(E) \propto \sum_{if} |M_{if}|^2 \delta(E_f + E_{He} - E_1 - E_2) \times \delta(E - E_f)$$

where the sum is on all pairs of two-electron initial and final states that satisfy energy conservation. If, contrary to the discussion of the previous paragraph, the matrix element is replaced by an isotropic average value, equation 5 can be reduced to

$$N(E) \propto \int \langle M \rangle \rho(E_1) \langle M \rangle \rho(E + E_{He} - E_1) dE_1$$

which is the self-convolution of the total density of states weighed by an average transition probability.

As a crude approximation, take the perturbing potential in equation 1 to be perfectly localized at the He^+ center. Then it is easily shown that

$$\langle |M_{if}|^2 \rangle \propto |\Psi_1(r = s)|^2 |\Psi_2(r = s)|^2$$

and thus the previous equation becomes the self-convolution of the local density of states

$$\rho(E,s) \equiv |\Psi_1(r = s)|^2 \rho(E_1)$$

evaluated at the center of the He^+ ion. Hagstrum has developed elaborate deconvolution procedures for unfolding observed spectra, $N(E)$ versus E, in order to obtain the local density of states (weighted by transition probabilities) for the single-electron process.

For information related to the single-electron spectrum of atoms to be extracted from an ion-neutralization spectrum, it is necessary that at least one of the electrons in the initial state be an extended Bloch state. If both electrons came from a localized state, or one atom, then the energy of the ejected electron would reflect the difference between E_{He} and the sum of the first and send ionization energies of the atom.

There are two examples taken from Hagstrum's[14] work that will illustrate the spatial localization of ion-neutralization spectroscopy. Figure 6 shows a comparison of ultraviolet-photoelectron spectroscopy and INS data for an ordered multilayer of tellurium on the (100) crystal face of nickel. We note several features: First, the very apparent Ni d-band peak at about −1 eV in $N_p(E)$ is greatly attenuated in the ion-neutralization spectrum; this is due to the two layers of Te that block the He^+ ion and thus do not allow it to overlap the Ni d-band wave-function tails. Second, the structure at about −3.8 eV is seen quite well in both spectra and compares with the energy of the p_z electrons in free Te. This is most likely a non-bonding orbital. On the other hand, the structure seen at −6.3 eV by UPS is barely resolved with INS. This could be the bonding orbital between the Te and Ni, which presumably is more tightly bound to the Te–Ni interface and thus does not project through the Te–vacuum interface to be felt by the He^+. Consequently its strength in the ion-neutralization spectrum is small.

When mercury is adsorbed on the Ni(100) surface, both ion-neutralization and ultraviolet photoelectron spectroscopy show two 5d, spin-orbit-split orbitals of Hg at the same energies. It can therefore be concluded that Hg is on the surface and not adsorbed into the surface region. This is in contrast with the case in which Hg is adsorbed on Si(111), because there the Hg orbitals are seen by ultraviolet photoelectron spectroscopy but not by INS; the simplest explanation for this is that the mercury atoms are adsorbed into the silicon surface.

Field-ionization spectroscopy

The first two vacuum-tunneling spectroscopies that we considered measure some property of the *occupied* electronic states at the surface. The third technique, field-ionization spectroscopy, allows us to measure properties of the *unoccupied* electronic states at the surface. Field-ion microscopy, which was developed by Müller,[15] uses noble-gas atoms that are ionized by the electric field at the surface of an emitter. The same geometry as that utilized for field emission images the atoms on a surface with atomic resolution. The energy spectrum of these ions can be analyzed with basically the same configuration as that shown in figure 2, where a probe hole in the screen is used to select the ions originating from a given region of the surface, which are subsequently energy analyzed. The technique in which the field-ion microscope is operated in this mode is referred to as field-ionization spectroscopy.

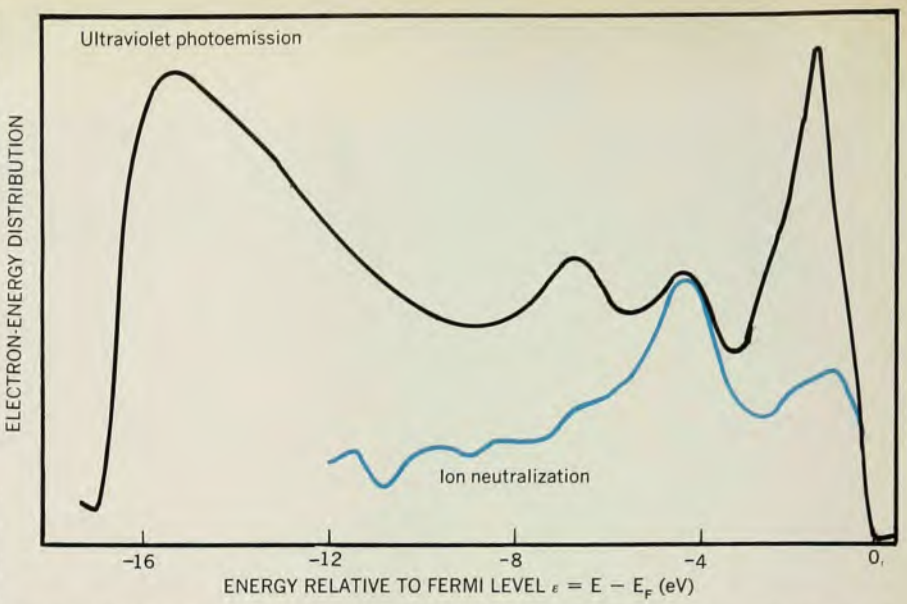

Two different methods, photoemission, N_p, and ion neutralization, U, show spectra emphasizing different features of Ni (100) with an ordered multilayer of tellurium. Figure 6

FIS is one of the few experimental methods that can provide direct information about the energy levels at the surface of a metal that lie above the Fermi energy but below the vacuum level. (However, FIS is not limited to energies below the vacuum level.) The more standard surface-sensitive techniques such as field emission, photoemission and ion-neutralization spectroscopy do not sample these levels.

In field-ionization experiments a strong electric field is applied to the sample with a polarity such that an electron outside the metal is driven towards it. Mobile gas atoms introduced near the metal surface can consequently lose their electrons to the metal by tunneling to states above the Fermi energy.

The potentials appropriate to field ionization are shown in figure 1c. The potential of the metal, located in the region $z < 0$, is shown schematically. Outside the metal, the external electric potential and the atomic potential of the gas atom combine as indicated in the figure. Because of the electric potential the energy level of the electron on the gas atom is raised from E_a to $E_a + eFs$, where s is the distance of the gas atom from the metal surface. If $E_a + eFs$ lies above the Fermi energy of the metal, an electron on the gas atom can tunnel into the metal. The resultant gas ion will then be accelerated away from the surface. The energy this ion has when it is collected depends on the distance of the atom from the surface when ionization took place.

The resultant ion energy distribution is directly related to the distribution of electronic states in the metal, because the probability for an atom to ionize at a particular distance from the surface is directly proportional to the number of metal states available to the tunneling electron. The ion current is given by

$$j(\epsilon) = (2\pi/\hbar)\sum_f \left|\int d^3r \Psi_f(\mathbf{r})\gamma(z)\right|^2 \delta(\epsilon - \epsilon_f) \quad (5)$$

where Ψ_f, ϵ_f denote the wave function and energy of the final state in the tunneling process (figure 1c). The function $\gamma(z)$ is large only for $z \approx s$ (figure 1c). As a rough approximation equation 5 can be written as

$$j(\epsilon) = c\sum_f \left|\Psi_f(\mathbf{s})\right|^2 \delta(\epsilon - \epsilon_f) \quad (6)$$

where c is a constant and $\mathbf{s}$ is the position of the ion.

Equation 6 tells us that field-ionization spectroscopy measures the density of metal states Ψ_f at the ion. Thus FIS experiments complement field-emission spectroscopy experiments in that FES measures the density of metal states near the surface at energies below the Fermi energy while FIS measures the density of metal states near the surface at energies above E_F. However, the tunneling barrier in FES is roughly five times that in FIS. Because of the very large barrier in FES only electrons with momentum normal to the metal surface contribute to the tunneling current whereas in FIS electrons with a rather wide range of momenta contribute to the current. This means that field-ion energy distributions from different surfaces of the same material can sample common regions of wave-vector space and may consequently show similar structure.

A recent field-ionization spectroscopy experiment with sufficient resolving power to yield information about the density of states was carried out by Takao Utsumi and Neville Smith[16] on surfaces of tungsten, both clean and

covered with nitrogen adsorbate. The resulting energy distributions exhibit a great deal of structure reflecting the complex energy bands of tungsten, and indicate great promise for identifying the unfilled localized states formed in chemisorption.

The above discussion, though simplified in many places, illustrates the general characteristics of vacuum-tunneling spectroscopy. In all the cases we have described, an electron must tunnel through a vacuum barrier, either into or out of the metal substrate. The measured current is therefore very sensitive to the properties of the wave function in the barrier. If the shape of vacuum barrier is known, as it is in the field-emission and field-ionization spectroscopies, the barrier-tunneling characteristics can be removed from the data, leaving a well prescribed measure of the electronic properties of the surface.

We and workers in other laboratories are now using these techniques as a quantitative check on theoretical calculations of the electronic properties of surfaces, such as those described in the article by Schrieffer and Soven. Thus the extreme surface sensitivity of a vacuum-tunneling spectroscopy can be used very successfully in conjunction with a spectroscopy such as photoemission to add "depth perception."

References

1. R. Gomer, *Field Emission and Field Ionization* Harvard U.P., Cambridge, Mass., (1961).
2. E. W. Müller, Z. Physik **106,** 541 (1937).
3. R. H. Fowler, L. W. Nordheim, Proc. Roy. Soc. (London) **A119,** 173 (1928).
4. R. D. Young, Phys. Rev. **113,** 110 (1959).
5. J. W. Gadzuk, E. W. Plummer, Rev. Mod. Physics, **45,** 487 (1973).
6. W. B. Shepherd, W. T. Peria, Surf. Sci. **38,** 461 (1973).
7. N. J. Dionne, T. N. Rhodin, Phys. Rev. Lett., **32,** 1311, (1954).
8. D. R. Penn, E. W. Plummer, Phys. Rev. **B9,** 1216, (1974).
9. C. D. Duke, M. E. Alferieff, J. Chem. Phys. **46,** 923 (1967).
10. H. E. Clark, R. D. Young, Surf. Sci. **12,** 385 (1968); E. W. Plummer, R. D. Young, Phys. Rev. **B1,** 2088 (1970).
11. E. W. Plummer, A. E. Bell, J. Vac. Sci. Technol. **9,** 583 (1972); L. W. Swanson, A. E. Bell, Adv. Electron. Electron Phys. **32,** 194 (1973).
12. H. D. Hagstrum, Science, **178,** 275 (1972); Phys. Rev. **96,** 336, (1954).
13. H. D. Hagstrum, G. E. Becker, Phys. Rev. Letters, **22,** 1054 (1969).
14. H. D. Hagstrum, Welch Award Address, J. Vac. Sci. Technol. **12,** 7 (1975).
15. E. W. Müller, T. T. Tsong, *Field Ion Microscopy: An Introduction to Principles, Experiments, and Applications,* American Elsevier, New York, (1969).
16. T. Utsumi, N. V. Smith, Phys. Rev. Lett., **33,** 1294, (1974). □